Showcasing research from Professor Yu-Ching Huang's laboratory, Department of Materials Engineering, Ming Chi University of Technology, New Taipei City, Taiwan.

Insights into the photovoltaic mechanism of organic photovoltaics under solar and artificial light

The photovoltaic performance of organic photovoltaics is determined by multiple factors. This work elucidates how these influencing factors differentially impact the performance of the organic photovoltaics under solar and indoor light illumination and paves the way for future applications of polymer solar cells in different fields.

As featured in:

See Yu-Ching Huang and Chia-Feng Li, *J. Mater. Chem. C*, 2023, **11**, 14088.

ROYAL SOCIETY OF CHEMISTRY

rsc.li/materials-c

Registered charity number: 207890

Journal of Materials Chemistry C

ROYAL SOCIETY OF CHEMISTRY

PAPER

View Article Online
View Journal | View Issue

Cite this: J. Mater. Chem. C, 2023, 11, 14079

Insights into the photovoltaic mechanism of organic photovoltaics under solar and artificial light†

Yu-Ching Huang *[abc] and Chia-Feng Li[a]

Received 5th July 2023,
Accepted 22nd September 2023

DOI: 10.1039/d3tc02372a

rsc.li/materials-c

Indoor organic photovoltaics (OPVs) have attracted a lot of attention due to their low energy consumption for applications such as Internet of Things (IoT) and wearable technology. However, the mechanisms influencing the indoor power conversion efficiency (PCE) of OPVs are not very well understood. In this study, we investigated how the active layer based on different acceptor materials, fullerene and non-fullerene, affects the performance of the device. Under indoor light, the optimal thickness of non-fullerene-based OPVs (PBDB-T:ITIC) is 140 nm with a PCE of 19.74% and the optimal thickness of fullerene-based OPVs (PBDB-T:$PC_{71}BM$) is 100 nm with a PCE of 16.22%. Our study systematically investigated the electrical performance and carrier behavior of different active layers under two light sources (1-Sun and indoor light). We found that the indoor PCE of the non-fullerene system is less affected by the thickness, mainly because the thicker non-fullerene active layer film still maintains good series resistance (R_s), shunt resistance (R_{sh}), and less charge recombination. Our study points out that the key factors affecting the indoor PCE of OPVs are R_{sh}, monomolecular recombination, and trap depth, revealing new insights into achieving high indoor PCE of OPVs.

Introduction

Organic photovoltaics (OPVs) have shown great potential in a wide range of applications such as portable and wearable electronics, building-integrated photovoltaics (BIPVs), and off-grid power generation due to their advantages of light weight, mechanical flexibility, semi-transparency, and low manufacturing cost.[1–5] Recently, the power conversion efficiency (PCE) of OPVs has reached over 18%,[6–8] and the highly efficient OPVs have mainly relied on the development of various non-fullerene acceptors (NFAs).[9–11] Compared with conventional fullerene derivatives as acceptor materials, NFAs synthesized by flexible molecular design can provide tunable energy bands and broad absorption regions, which are more suitable for the current innovative donor polymers.[12–14] Despite the progress achieved for OPVs, OPVs still need to overcome many technical bottlenecks, such as large-area fabrication and operational stability, to compete with commercial grid-connected Si-based PV systems.

In recent years, due to the emergence of Internet of Things (IoT) technology, low energy-consuming electronics, such as wireless sensors and router nodes, can have their key components powered by the tiny energy generated by indoor light, creating a niche market for OPVs. Previous studies have pointed out that OPVs exhibit higher indoor PCE than inorganic photovoltaics[15,16] due to their characteristics of highly adjustable light absorption and low current leakage. Currently, the indoor PCE of OPVs can reach over 30%,[17,18] demonstrating the great potential of OPVs for integrating low-energy-consuming electronics in indoor applications. The light source is the major difference between indoor and outdoor power generation. Compared to outdoor sunlight, which has a fixed emission spectrum and intensity, indoor artificial light sources have diverse emission spectra (mainly in the visible light region) and much lower intensity (less than one-thousandth of that of sunlight). The high indoor PCE of OPVs results from that OPVs can adjust the absorption range to match various indoor light sources by selecting appropriate materials. Several research groups have revealed different PV behaviors and mechanisms under solar and indoor light and provided useful suggestions for improving the indoor PCE of OPVs. C. J. Brabec's research team investigated the effects of series resistance (R_s) and shunt resistance (R_p) on the PCE of OPVs

[a] Department of Materials Engineering, Ming Chi University of Technology, New Taipei City 24301, Taiwan. E-mail: huangyc@mail.mcut.edu.tw
[b] Organic Electronics Research Center, Ming Chi University of Technology, New Taipei City 24301, Taiwan
[c] Biochemical Technology R&D Center, Ming Chi University of Technology, New Taipei City 24301, Taiwan

† Electronic supplementary information (ESI) available: Additional *J–V* measurements, characteristics of devices, absorption spectrum, morphology, and photovoltaic characteristics of devices. See DOI: https://doi.org/10.1039/d3tc02372a

under outdoor (1-Sun) and indoor conditions. Their results indicated that a high R_p is required and R_s is less important for the indoor PCE of OPVs, which is in contrast to the 1-Sun PCE.[19] W. C. Choi *et al.* demonstrated the indoor PCE of OPVs fabricated from three polymers blended with fullerenes. They indicated the importance of open-circuit voltage (V_{OC}) for the indoor PCE and suggested that systems for indoor applications should not be selected with only the 1-Sun PCE of OPVs.[20] F. C. Chen *et al.* studied several polymer blends and concluded that increasing V_{OC} is a key factor in achieving the high indoor PCE of OPVs.[21] Their results suggest that the photocurrent is not critical for indoor PCE because the OPVs already have a high ability to harvest the photons in the relatively narrow visible spectrum of the indoor light. In addition, W. C. Tsoi *et al.* tuned the morphological changes of the active layer consisting of small molecules and fullerenes using a solvent vapor annealing process, and they explored the effect of morphology on the optoelectronic properties of the OPVs.[22] Their results showed that the effect of film morphology on the PCE was weaker under indoor light than under 1-Sun. T. Yasuda *et al.* suggested that the mutual match between the photoabsorption response of the indoor OPVs and the illumination spectra of the artificial light sources is also a possible reason for the improved indoor PCE. Their results indicated that the indoor PCEs of OPVs change with the color temperature of incident LED illumination.[23] J. Y. Kim *et al.* designed three semi-crystalline polymers to verify the effect of different molecular stackings on indoor PCE. Their results implied that OPVs can be used for indoor applications as long as R_{sh} is high enough. Additionally, the crystal morphology is a major parameter in designing an ideal indoor PV molecule to increase the R_{sh} of OPVs.[24] H. Yan *et al.* investigated the effect of electron transport layers (ETLs) on the indoor PCE. Their results indicated that OPVs with a band-aligned interlayer exhibit a significant low leakage current and trap-assisted recombination, which in turn improves the indoor PCE.[25] Although several studies have presented the influencing factors in the indoor PCE, such as the shunt resistance, V_{OC}, film morphology, inner nanostructure, artificial light illumination spectrum, and interfacial band-alignment, most of the literature still focuses on the improvement of 1-Sun PCE, while the indoor PCE is only additional data. Therefore, in-depth investigations on the power conversion mechanism under indoor light are still relatively lacking.

Because the relationship between charge density and light intensity is linear, both leakage current and defect-assisted recombination are more pronounced when the carrier density is low under indoor light.[25–27] Our previous study demonstrated that trap-assisted recombination dominates in PSCs under indoor light.[28] Therefore, the well-controlled recombination behavior is very important to improve the indoor PCE of OPVs. In OPVs, defects between the donor and acceptor materials are the main cause of trap-assisted recombination. Previous literature reported that the use of fullerene derivatives and non-fullerene materials as acceptor materials improves the indoor PCE of OPVs. S. S. Yang *et al.* evaluated the effect of different fullerene derivatives as acceptor materials on the indoor PCE of OPVs (TL5, 500 lux).[21] Their results indicated that the use of the fullerene derivative with a higher lowest unoccupied molecular orbital (LUMO) energy level can exhibit a higher V_{OC} (0.89 V) with an indoor PCE over 13%. Y. Cui *et al.* obtained a high PCE of 24.6% under indoor illumination (LED, 500 lux) using a NFA with a large energy gap and low energy loss.[29] For subsequent potential material combinations for high-performance indoor OPVs, some important material combinations for high-V_{OC} OPVs have been revealed in the literature.[30–32] These studies mainly focused on the effect of the energy level between fullerene derivatives and NFAs on the indoor PCE of OPVs; however, the different carrier behaviors of OPVs based on the two acceptor materials under indoor light remain unclear.

In this study, we used a donor material, PBDB-T, with two acceptor materials, a spherical fullerene derivative ($PC_{71}BM$) and a linear NFA (ITIC), as the active layer of PSCs, respectively. We observed the nanostructures, film morphology and crystallinity in the PSCs based on these two active layer systems and investigated the different carrier behaviors under indoor light.

Experimental method

Materials

Zinc acetate dihydrate (99%), 2-methoxyethanol (99.8%), ethanolamine (99.5%), ethanol (99.8%), chlorobenzene (CB, 99.8%), 1,8-diiodooctane (DIO, 98%), and molybdenum(VI) oxide (MoO_3, 99.5%) were purchased from Sigma Aldrich. PBDB-T and ITIC were obtained from 1-Material, and $PC_{71}BM$ and indium tin oxide (ITO) coated glasses with a sheet resistance of 15 $\Omega\ \square^{-1}$ were purchased from Lumtec Corporation. The chemical structure of the active layer materials is shown in Fig. S1 (ESI†).

Device fabrication

In this study, we fabricated inverted OPVs with the following device structure: ITO/ZnO/active layer/MoO_3/Ag. Sol–gel ZnO and MoO_3 were used as the electron transport layer (ETL) and hole transport layer (HTL), respectively. The cleaning procedure of the ITO transparent electrode, the deposition of the sol–gel ZnO film, and the evaporation process of MoO_3 and Ag are described in our previous literature.[28] The active layers used in this study were from PBDB-T:ITIC and PBDB-T:$PC_{71}BM$. The solutions of PBDB-T:ITIC and PBDB-T:$PC_{71}BM$ were prepared by dissolving donor and acceptor materials (1 : 1, 20 mg mL^{-1}) in CB and adding 0.5 vol% DIO and 3 vol% DIO as additives, respectively.

Characterization

The 1-Sun and indoor *J–V* curves of the OPVs were measured separately using an AM 1.5G solar simulator (Enlitech, SS-X100R AAA) and the indoor *I–V* characteristics of OPVs (ITRI). The thickness of active layers was obtained using a 3D optical profiler (Bruker, Contour Elite). The absorbance of the active layers was measured using a UV-vis spectrometer (JASCO, V-730). Steady-state photoluminescence (PL) spectra

were recorded using a fluorescence spectrophotometer (HORIBA, FluoroMax 4). The surface morphology of the films was studied using atomic force microscopy (AFM) (Bruker, Innova). Transient photovoltage (TPV) and photocurrent (TPC) measurements were performed using an all-in-one characterization platform (Paios, Fluxim AG, Switzerland). Electrochemical impedance spectra (EIS) were recorded using an impedance measurement unit (AMETEK Scientific Instruments, Material Lab XM), and the Nyquist plots were obtained from 1 MHz to 10 Hz at applied voltages set to device open-circuit voltages.

Results and discussion

The PCE of the devices under different light illumination is first determined by the mutual matching of the emission spectrum of the light source and the absorption of the active layers. The absorption of the devices is strongly influenced by the thickness of the active layers; therefore, we first investigate the effect of film thicknesses on the absorption behavior. Fig. S2(a) and (b) (ESI†) illustrate the absorption spectra of the active layers of different thicknesses fabricated from PBDT-T:$PC_{71}BM$ and PBDT-T:ITIC, respectively. The absorption region of both systems is around 400–700 nm, which coincides with the emission spectrum of the indoor light TL 84,[33] and the higher absorption intensity is performed with the thicker active layers in both systems. Although thicker films can absorb more light, which may improve the short-circuit current (J_{SC}), it may also lead to lower FF due to poor charge transport and increased charge recombination. The PL of these thin films can be utilized to study the exciton dissociation behavior of active layers of different thicknesses. Fig. S2(c) and (d) (ESI†) show the PL spectra of these films and the results indicate that in both systems, exciton dissociation can be effectively generated upon the incorporation of the acceptor materials. However, both systems exhibit poor exciton dissociation when the thickness of the active layer increases to 160 nm, a phenomenon that is more pronounced in the non-fullerene system. The poor exciton dissociation implies a lower effective charge generation, which may lead to a decrease in the J_{SC} and FF of the device. We also measured the morphology of the active layers to clarify the interfacial contact between the active layer and the HTL. According to the surface morphology shown in Fig. S3 (ESI†), the root-mean-square (RMS) surface roughness of the PBDB-T:$PC_{71}BM$ films slightly increased from 2.35 nm to 3.33 nm as the film thickness increased from 65 nm to 160 nm. In contrast, the RMS surface roughness of the PBDB-T:ITIC films increased from 1.91 nm to 6.49 nm with a similar thickness change. In the case of the non-fullerene system, increasing the film thickness leads to a rougher surface morphology, implying ineffective charge transport and increased charge recombination due to the poor interfacial contact between the active layer and the HTL, which is consistent with the PL results.

The *J–V* curves of the devices fabricated from PBDB-T:$PC_{71}BM$ and PBDB-T:ITIC under two light illumination sources, 1-Sun and TL84 (200 lux), are shown in Fig. S4 (ESI†) and the related photovoltaic characteristics are listed in Tables S1 and S2 (ESI†). We named the PCEs illuminated under 1-Sun and TL84 as 1-Sun PCE and indoor PCE, respectively. The highest 1-Sun PCEs of devices based on PBDB-T:$PC_{71}BM$ and PBDB-T:ITIC are 6.93% and 9.50%, respectively, with optimal active layer thicknesses of 100 nm for both systems. When the devices are illuminated under TL84 at 200 lux, the optimal thicknesses of the active layers are 100 nm and 140 nm, respectively. Fig. 1 shows that the 1-Sun and indoor PCEs of these devices varied with the thickness of the active layer. In the

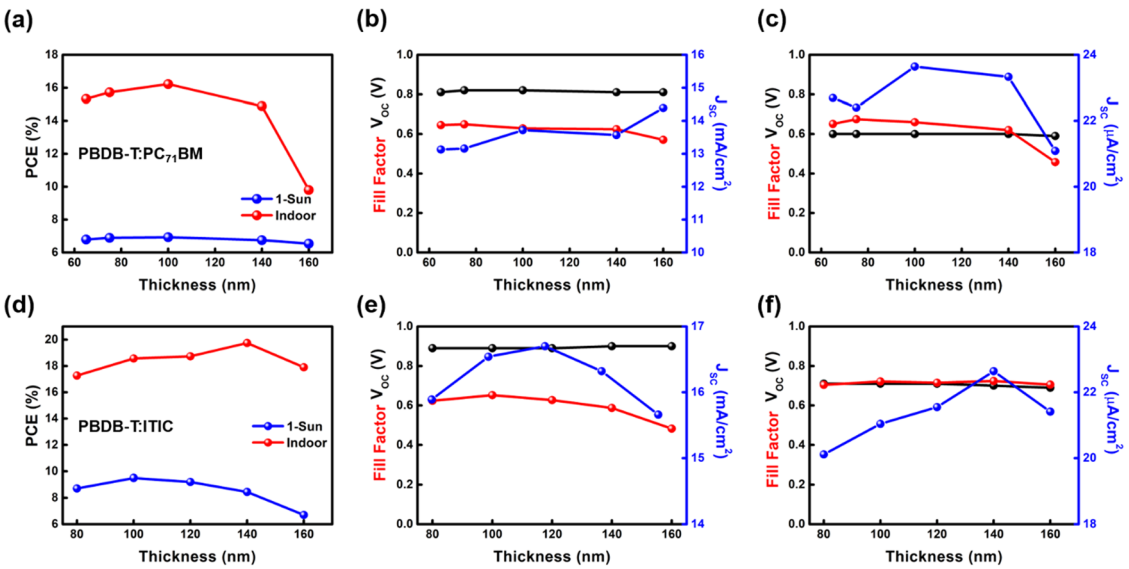

Fig. 1 Variation of performance with the active layer thickness under different light illumination sources. PBDB-T:$PC_{71}BM$-based devices: (a) PCE variation, and V_{OC}, J_{SC}, and FF variations under (b) 1-Sun and (c) TL84 (200 lux). Devices based on PBDB-T:ITIC-based devices: (d) PCE variation, and V_{OC}, J_{SC}, and FF variations under (e) 1-Sun and (f) TL84 (200 lux).

PBDB-T:$PC_{71}BM$ system, the 1-Sun PCEs of the devices are less affected by the film thickness. From the photovoltaic properties, we can see that the similar 1-Sun PCEs of devices based on PBDB-T:$PC_{71}BM$ are due to a trade-off between increasing J_{SC} and decreasing FF with the increasing active layer thickness. In contrast, the 1-Sun PCEs of devices based on PBDB-T:ITIC decrease with the increasing thickness of the active layer because of the simultaneous reduction in J_{SC} and FF. Fig. S5 (ESI†) shows the EQE spectra and the integrated J_{SC} measured in the wavelength range from 300 nm to 900 nm. It is noteworthy that the trend of the indoor PCEs of these two devices with the active layer thickness is in contrast to the trend of 1-Sun PCEs. The indoor PCEs of PBDB-T:$PC_{71}BM$-based devices considerably decrease with the increasing active layer thickness, but the indoor PCEs of PBDB-T:ITIC-based devices remain almost unchanged with the active layer thickness. This result implies that fullerenes- and non-fullerenes-based active layers have different influences on the 1-Sun and indoor PCEs of these devices. Moreover, we revealed the photostability of PBDB-T:ITIC devices with different thicknesses under continuous illumination from different light sources. As shown in Fig. S6 (ESI†), the photostability of the devices illuminated under indoor light is better than that under 1-Sun irradiation. However, the photostability of devices with different thicknesses of the active layers performs differently, and the thin-film OPVs exhibit better photostability than the thick-film OPVs under the two light sources. Previous studies have indicated that the photodegradation of OPVs is mainly caused by the bulk and interfacial defects in the film,[34] which implies the reason why the thick-film OPVs exhibit poorer photostability.

We further observed the variation of series resistance (R_s) and shunt resistance (R_{sh}) under different light sources (Fig. 2) and are listed the calculated values in Table S3 (ESI†). In general, devices with high PCE should exhibit low R_s and high R_{sh}. In the PBDB-T:$PC_{71}BM$ system, the trends of R_s and R_{sh} are consistent with the PCE variations regardless of 1-Sun and TL84. The lowest R_s and highest R_{sh} are obtained with a film thickness of 100 nm, and the indoor PCE can reach 16.22%. However, in the PBDB-T:ITIC system, the trends of R_s and R_{sh} under TL84 are different from those under 1-Sun. From this result, we infer that the indoor PCE of the OPVs fabricated from PBDB-T:ITIC can still be maintained with the increasing active layer thickness, which is mainly due to the improvement of R_s and R_{sh} for the thicker active layer. The highest indoor PCE of 19.74% can be achieved as the film thickness is 140 nm. It is particularly noteworthy that in the PBDB-T:ITIC system (high V_{OC}), the R_{sh} under TL84 is greater than that of the PBDB-T:$PC_{71}BM$ system (low V_{OC}). Our results verify that the R_{sh} of the devices under indoor light has a greater impact on the indoor PCE than R_s. However, as the R_s of the devices under indoor light exceeds 5 KΩ cm^2, the effect of R_s on the indoor PCE becomes non-negligible. From our results, we can conclude that good indoor PCE can be obtained when we control the indoor OPVs with R_s less than 5 KΩ cm^2 and R_{sh} greater than 450 KΩ cm^2.

Moreover, we investigated the charge recombination behaviors, including monomolecular and bimolecular recombination, of these devices under different light illumination by measuring the variation of V_{OC} and J_{SC} with light intensity, respectively. Monomolecular recombination, also known as trap-assisted recombination, refers to the recombination of

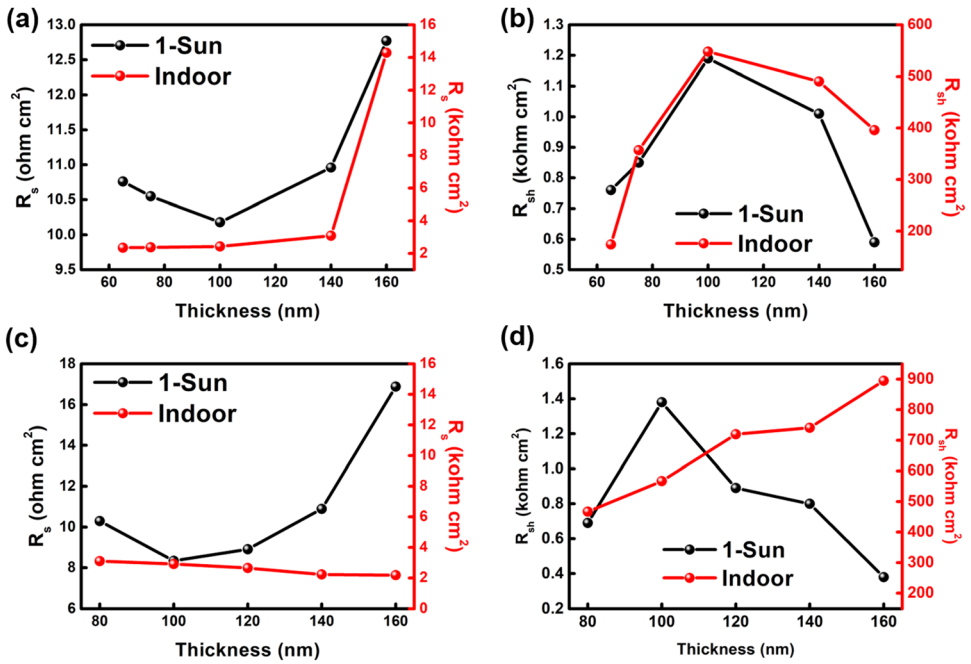

Fig. 2 Variation of series resistance (R_s) and parallel resistance (R_{sh}) of the devices under 1-Sun and TL84. (a) R_s and (b) R_{sh} of PBDB-T:$PC_{71}BM$. (c) R_s and (d) R_{sh} of PBDB-T:ITIC.

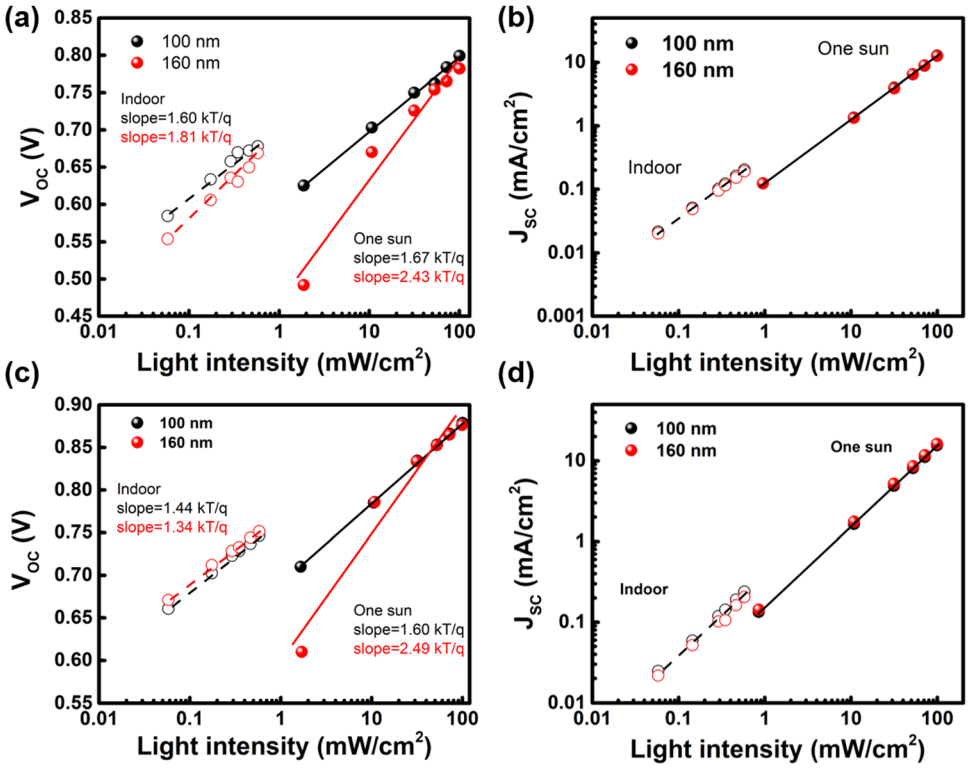

Fig. 3 Light intensity dependence of V_{OC} and J_{SC} of the OPVs with different active layer thicknesses under 1-Sun and indoor light. (a) and (b) PBDB-T:$PC_{71}BM$-based OPVs. (c) and (d) PBDB-T:ITIC based OPVs.

electrons and holes induced by the traps during electron and hole transport to their electrodes.[35–37] As the value of n approaches 1, monomolecular recombination is inhibited. Bimolecular recombination is another recombination behavior that is not captured by the trap state. When the value of α is close to 1, the bimolecular recombination in the system is almost negligible. From Fig. 3, the monomolecular recombination under l-Sun for both active systems becomes severe as the thickness of the active layer increases. Under indoor light illumination, the monomolecular recombination in PBDB-T:$PC_{71}BM$-based devices still becomes apparent with increasing thickness. In contrast, the PBDB-T:ITIC-based devices exhibit suppressed monomolecular recombination at the thick active layer. In addition, the trend of bimolecular recombination with the thickness was almost the same for both active layer systems under 1-Sun and indoor light. Our results suggest that the monomolecular recombination behavior under indoor light may be an important key factor affecting the indoor PCE of the PBDB-T:ITIC-based devices.

We further observed the carrier lifetime and carrier extraction time of devices under different light illumination by using TPV and TPC. Fig. 4 shows the results of TPV and TPC for devices with different thicknesses at different light intensities, and the corresponding carrier lifetime and extraction time are listed in Table S4 (ESI†). We can obtain the carrier lifetime at a fixed bias voltage from TPV.[38] At a light intensity of 100 mW cm^{-2}, the carrier lifetime of devices fabricated from PBDB-T:$PC_{71}BM$ decreased from 13.74 ms to 6.46 ms when the active layer thickness was increased from 100 nm to 160 nm. This result implies that the thick fullerene-based active layer exhibits increasing defects in the BHJ structure, which in turn leads to an increase in molecular recombination. This result is also consistent with the previous decreasing trend of J_{SC} and FF. However, in the PBDB-T:ITIC system, the increasing thickness of the active layer does not cause an obvious change in the carrier lifetime (from 14.43 ms to 14.06 ms), which implies that the defects in the BHJ structure of the PBDB-T:ITIC film do not increase when the thickness of the active layer increases. For the devices illuminated under low light intensity, the variation in the carrier lifetime is similar to that in the high light intensity, indicating that the thickness variation has more impact on the fullerene system than that on the non-fullerene system. The carrier extraction time increases with the increasing thickness for both fullerene and non-fullerene systems. This result suggests that the increasing thickness of the active layer is not favorable for carrier extraction. However, it can be deduced from the indoor PCE that the difference in extraction time is not the main affecting factor in the indoor PCE.

To further understand the interfacial behavior of OPVs under different light sources, we measured the interfacial impedance of the two systems separately by using impedance spectroscopy. Fig. 5 shows the Cole–Cole plot of the two OPVs under different light sources, representing the relationship between the real and imaginary parts of the device resistance and the change in frequency. Using the equivalent circuit in Fig. 5(a), the fitted data are listed in Table S5 (ESI†). R_s is the

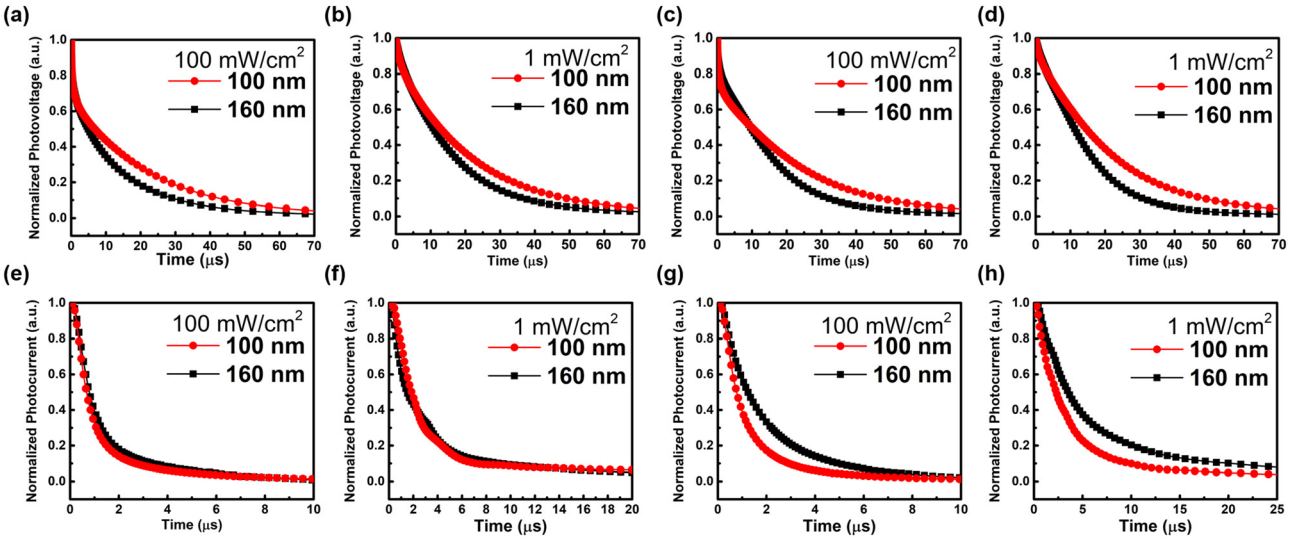

Fig. 4 Normalized TPV of devices with different active layer thicknesses under two light intensities: (a) and (b) PBDB-T:$PC_{71}BM$ and (c) and (d) PBDB-T:ITIC. Normalized TPC of devices with different active layer thicknesses under two light intensities: (e) and (f) PBDB-T:$PC_{71}BM$ and (g) and (h) PBDB-T:ITIC.

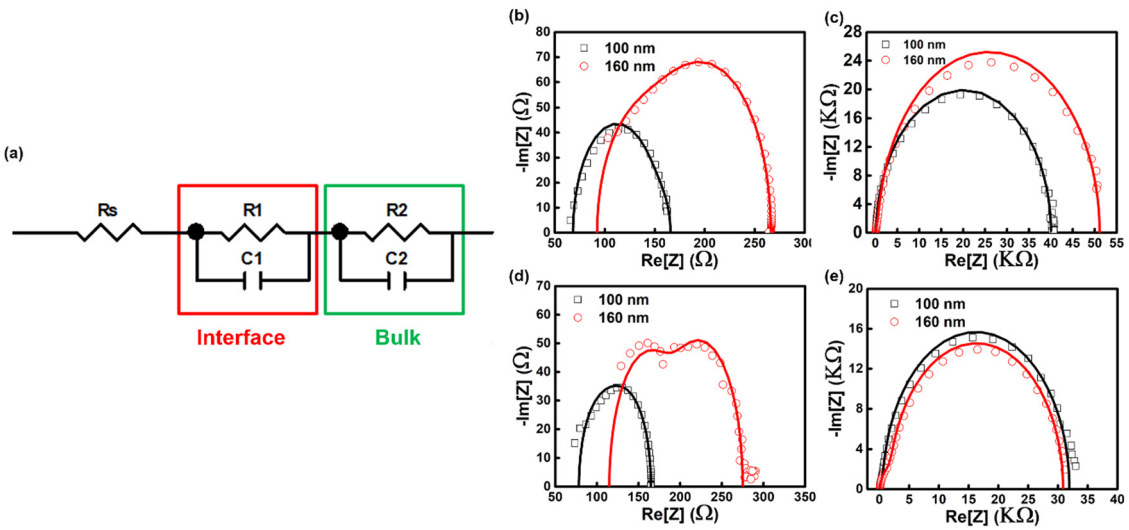

Fig. 5 (a) Equivalent circuit used to analyse the impedance data. The Cole–Cole diagram of PBDB-T:$PC_{71}BM$-based OPVs under (b) 1-Sun and (c) indoor light (TL84, 200 lux), and PBDB-T:ITIC-based OPVs under (d) 1-Sun and (e) indoor light (TL84, 200 lux).

series resistance, the shunt pairs with $R1$ and $C1$ refer to the complex resistance and capacitance at the interface between the active layer and the carrier transport layer, and the shunt pairs with $R2$ and $C2$ represent the charge transfer resistance and diffusion capacitance of the BHJ structured active layer. From these results, the R_s and $R1$–$C1$ shunt pairs of the PBDB-T:$PC_{71}BM$ and PBDB-T:ITIC-based OPVs become larger with the increasing thickness under different light illumination sources, representing no major difference in the trend of R_s and the interfacial resistance between the two kinds of devices under 1-Sun and indoor light. Noteworthy is the change in the $R2$–$C2$ shunt pair of the two BHJ structured active layers under the two light illumination sources. Firstly, both systems show unsmooth semicircular curves under 1-Sun illumination, indicating that there is more than one pair of resistance–capacitance–shunt in the equivalent module, possibly from the combination of shunt pairs at the interfaces between the acceptor and donor in the active layers. Under indoor light, the smoother semicircular curves indicate that there are fewer shunt pairs at the acceptor/donor interfaces in the active layers. In addition, the large semicircle represents the high resistance of the BHJ structured active layer, in which resistance increases with the active layer thickness for both systems under 1-Sun illumination. However, the PBDB-T:ITIC system is less affected by the thickness under indoor light irradiation, which may be due to the existence of a good acceptor/donor interfaces for effective charge transfer. This result demonstrates the importance of a well-mixed acceptor/donor interface in the BHJ

structured active layers under indoor light. The impedance of the BHJ structured active layers fabricated from non-fullerene acceptors does not change significantly with the thickness of the active layer, which is the main reason why the non-fullerene based OPVs are able to maintain a high indoor PCE.

Finally, we systematically investigated the trap depth and charge accumulation behavior of two different active layer systems. Fig. 6(a) and (b) show the J_{SC} measured at different temperatures, from which the trap depth of the devices can be calculated.[28] The trap depths of the PBDB-T:$PC_{71}BM$-based PSCs are deeper than those of PBDB-T:ITIC-based PSCs under both solar and indoor light illumination. The deeper trap depth implies that these would be more recombination centres in the active layer, leading to high carrier recombination efficiency detrimental to the PCE. Fig. 6(c) and (d) show the chemical capacitance–voltage relationship extracted from the EIS measurements, and the fitted straight lines indicate the occupied density of state (DOS),[39,40] which can be used to analyse changes in the effective energy level. Our previous literature has pointed out that the shift in voltage is proportional to the effective bandgap shift.[41] Compared to fullerene-based PSCs, NFA-based PSCs can obtain larger V_{OC} values under both solar and indoor light, which can be attributed to their larger effective energy level dispersion.[42–44] Furthermore, by measuring the capacitance change of the device at different applied voltages, the shift of the light intensity against the V_{peak} value can be used to deduce the extent of photogenerated carrier accumulation. Fig. 7 illustrates the V_{peak} shifts of the two active layer systems under 1-Sun and indoor light. The lower offset values imply less charge accumulation, which may correspond to high carrier mobility. When the devices are illuminated by indoor light, we found that V_{peak} almost unchanged with the decreasing intensity of indoor light illumination. This result implies that the charge accumulation is now not obvious under indoor light, and we speculate that this is related to the lower number of carriers generated under indoor light. In addition, we measured the carrier mobility using the charge extraction of photogenerated charge carriers by linearly increasing the voltage (Photo-CELIV).[45] The corresponding photocurrent curves and the calculated average mobilities are shown in Fig. S7 and Table S6 (ESI†), respectively. The results indicate that the carrier mobilities of the two systems are relatively different under 1-Sun illumination. When the light intensity decreases from 100 mW cm^{-2} to 1 mW cm^{-2}, the mobilities of the two systems increase and are relatively close to each other. This result is in agreement with the V_{peak} shift result. We can conclude that the difference in PCE between fullerene-based and NFA-based PSCs under 1-Sun can be attributed to the difference in the trap depth and carrier mobility, resulting in charge recombination and accumulation in the active layer. However, the charge accumulation in both systems was not significant under indoor light. Our result shows that the trap depth affects the carrier recombination rate, which is the main factor affecting the indoor PCE of OPVs.

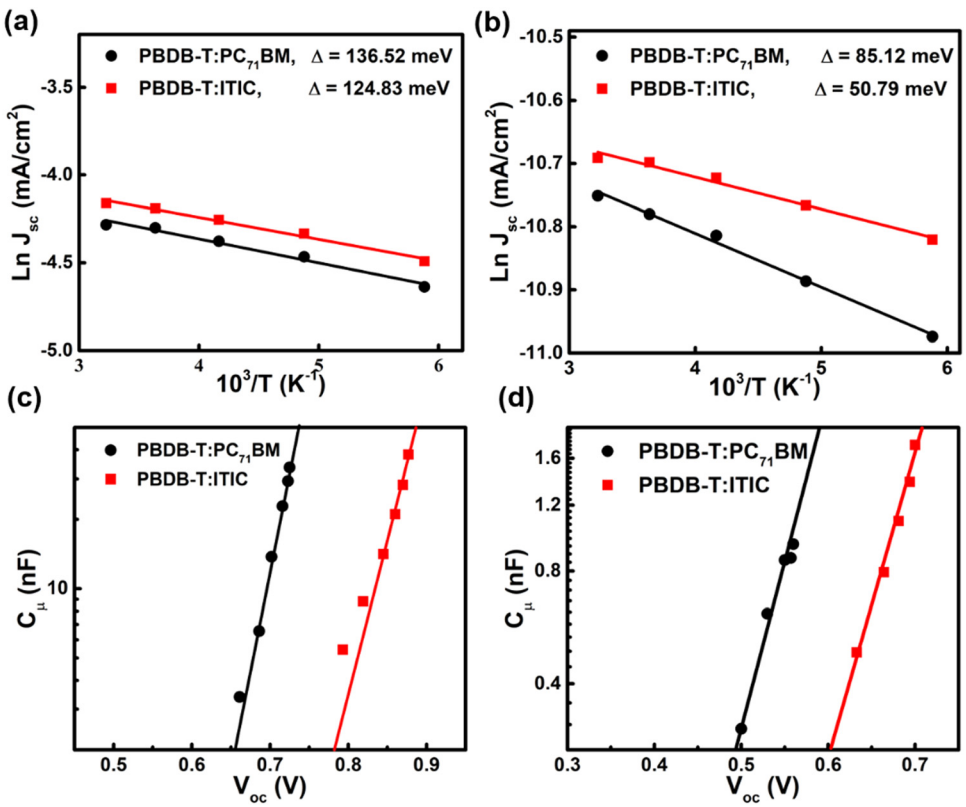

Fig. 6 The calculated trap depth under (a) 1-Sun and (b) indoor light (TL84, 200 lux). The capacitance under (c) 1-Sun and (d) indoor light (TL84, 200 lux).

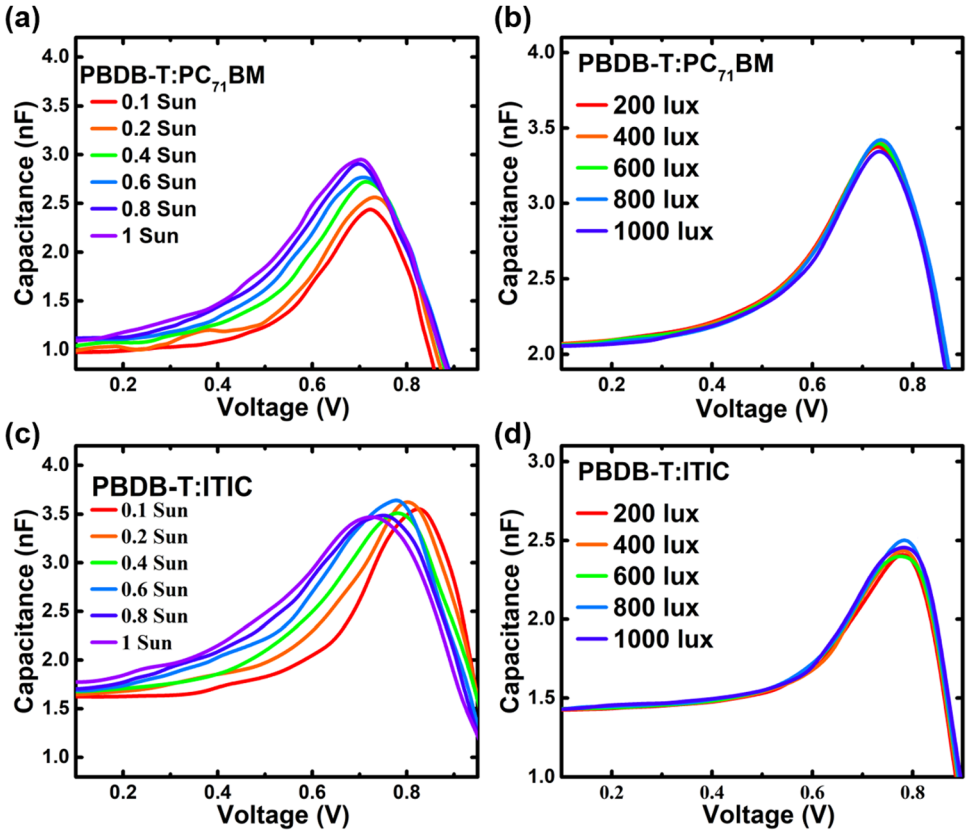

Fig. 7 Capacitance–voltage plots measured at room temperature and at various light intensities: PBDB-T:$PC_{71}BM$-based OPVs were illuminated under (a) 1-Sun and (b) indoor light (TL84). PBDB-T:ITIC-based OPVs were illuminated under (c) 1-Sun and (d) indoor light (TL84).

Conclusions

In conclusion, we found that a thicker active layer leads to a decrease in both 1-Sun and indoor PCEs in the PBDB-T:$PC_{71}BM$ system. In the PBDB-T:ITIC system, thicker active layers reduce the 1-Sun PCE of OPVs, which is consistent with the exciton dissociation and morphology measurements performed using PL and AFM, respectively. However, thicker active layers based on the PBDB-T:ITIC system do not reduce the indoor PCE of OPVs. The main reason is the improvement of the high shunt resistance and monomolecular recombination behavior of the devices with increasing film thickness. Our study indicates that the key factors for obtaining high indoor PCEs are R_s less than 5 KΩ cm^2 and R_{sh} greater than 450 KΩ cm^2. Moreover, the control of carrier recombination behavior, especially monomolecular recombination and trap depth, improves the indoor PCE of OPVs.

Author contributions

Y. C. H.: conceptualization, resources, supervision, funding acquisition, methodology, and writing – review and editing. C. F. L.: data curation, formal analysis, investigation, visualization, and writing – original draft.

Conflicts of interest

There are no conflicts to declare.

Acknowledgements

Financial support provided by the National Science and Technology Council of Taiwan (Grant No. NSTC 112-2628-E-131-001-MY4, 111-2221-E-131-022, 110-2221-E-131-010, and 107-2218-E-131-007-MY3) is highly appreciated.

References

1 G. Dennler, M. C. Scharber and C. J. Brabec, *Adv. Mater.*, 2009, **21**, 1323–1338.
2 H. Kang, G. Kim, J. Kim, S. Kwon, H. Kim and K. Lee, *Adv. Mater.*, 2016, **28**, 7821–7861.
3 B. Lee, L. Lahann, Y. Li and S. R. Forrest, *Sustainable Energy Fuels*, 2020, **4**, 5765–5772.
4 Y. Sun, L. Meng, X. Wan, Z. Guo, X. Ke, Z. Sun, K. Zhao, H. Zhang, C. Li and Y. Chen, *Adv. Funct. Mater.*, 2021, **31**, 2010000.
5 Y.-M. Sung, M.-Z. Li, D. Luo, Y.-D. Li, S. Biring, Y.-C. Huang, C.-K. Wang, S.-W. Liu and K.-T. Wong, *Nano Energy*, 2021, **80**, 105565.

6 Q. Liu, Y. Jiang, K. Jin, J. Qin, J. Xu, W. Li, J. Xiong, J. Liu, Z. Xiao, K. Sun, S. Yang, X. Zhang and L. Ding, *Sci. Bull.*, 2020, **65**, 272–275.
7 J. Wang, Y. Cui, Y. Xu, K. Xian, P. Bi, Z. Chen, K. Zhou, L. Ma, T. Zhang, Y. Yang, Y. Zu, H. Yao, X. Hao, L. Ye and J. Hou, *Adv. Mater.*, 2022, **34**, 2205009.
8 L. Zhu, M. Zhang, J. Xu, C. Li, J. Yan, G. Zhou, W. Zhong, T. Hao, J. Song, X. Xue, Z. Zhou, R. Zeng, H. Zhu, C.-C. Chen, R. C. I. MacKenzie, Y. Zou, J. Nelson, Y. Zhang, Y. Sun and F. Liu, *Nat. Mater.*, 2022, **21**, 656–663.
9 Y. Cui, H. Yao, J. Zhang, K. Xian, T. Zhang, L. Hong, Y. Wang, Y. Xu, K. Ma, C. An, C. He, Z. Wei, F. Gao and J. Hou, *Adv. Mater.*, 2020, **33**, 1908205.
10 X. Ma, J. Wang, J. Gao, Z. Hu, C. Xu, X. Zhang and F. Zhang, *Adv. Energy Mater.*, 2020, **10**, 2001404.
11 J. Wang, Y. Wang, P. Bi, Z. Chen, J. Qiao, J. Li, W. Wang, Z. Zheng, S. Zhang, X. Hao and J. Hou, *Adv. Mater.*, 2023, **35**, 2301583.
12 J. Q. Zhang, H. S. Tan, X. G. Guo, A. Facchetti and H. Yan, *Nat. Energy*, 2018, **3**, 720–731.
13 G. Li, X. Zhang, L. O. Jones, J. M. Alzola, S. Mukherjee, L.-W. Feng, W. Zhu, C. L. Stern, W. Huang, J. Yu, V. K. Sangwan, D. M. DeLongchamp, K. L. Kohlstedt, M. R. Wasielewski, M. C. Hersam, G. C. Schatz, A. Facchetti and T. J. Marks, *J. Am. Chem. Soc.*, 2021, **143**, 6123–6139.
14 J. Yuan, Y. Zhang, L. Zhou, G. Zhang, H.-L. Yip, T.-K. Lau, X. Lu, C. Zhu, H. Peng, P. A. Johnson, M. Leclerc, Y. Cao, J. Ulanski, Y. Li and Y. Zou, *Joule*, 2019, **3**, 1140–1151.
15 C. L. Cutting, M. Bag and D. Venkataraman, *J. Mater. Chem. C*, 2016, **4**, 10367–10370.
16 R. Arai, S. Furukawa, Y. Hidaka, H. Komiyama and T. Yasuda, *ACS Appl. Mater. Interfaces*, 2019, **11**, 9259–9264.
17 C. Lee, J. H. Lee, H. H. Lee, M. Nam and D. H. Ko, *Adv. Energy Mater.*, 2022, **12**, 2200275.
18 P. Bi, C. An, T. Zhang, Z. Chen, Y. Xu, Y. Cui, J. Wang, J. Li, Y. Wang, J. Ren, X. Hao, S. Zhang and J. Hou, *J. Mater. Chem. A*, 2023, **11**, 983–991.
19 R. Steim, T. Ameri, P. Schilinsky, C. Waldauf, G. Dennler, M. Scharber and C. J. Brabec, *Sol. Energy Mater. Sol. Cells*, 2011, **95**, 3256–3261.
20 H. K. H. Lee, Z. Li, J. R. Durrant and W. C. Tsoi, *Appl. Phys. Lett.*, 2016, **108**, 5.
21 S. S. Yang, Z. C. Hsieh, M. L. Keshtov, G. D. Sharma and F. C. Chen, *Sol. RRL*, 2017, **1**, 6.
22 H. K. H. Lee, J. Y. Wu, J. Barbe, S. M. Jain, S. Wood, E. M. Speller, Z. Li, F. A. Castro, J. R. Durrant and W. C. Tsoi, *J. Mater. Chem. A*, 2018, **6**, 5618–5626.
23 R. Arai, S. Furukawa, N. Sato and T. Yasuda, *J. Mater. Chem. A*, 2019, **7**, 20187–20192.
24 S. Y. Park, Y. Li, J. Kim, T. H. Lee, B. Walker, H. Y. Woo and J. Y. Kim, *ACS Appl. Mater. Interfaces*, 2018, **10**, 3885–3894.
25 L.-K. Ma, Y. Chen, P. C. Y. Chow, G. Zhang, J. Huang, C. Ma, J. Zhang, H. Yin, A. M. Hong Cheung, K. S. Wong, S. K. So and H. Yan, *Joule*, 2020, **4**, 1486–1500.
26 J. S. Goo, S.-C. Shin, Y.-J. You and J. W. Shim, *Sol. Energy Mater. Sol. Cells*, 2018, **184**, 31–37.
27 Z. Chen, T. Wang, Z. Wen, P. Lu, W. Qin, H. Yin and X.-T. Hao, *ACS Energy Lett.*, 2021, **6**, 3203–3211.
28 Y.-M. Sung, A. K. Akbar, S. Biring, C.-F. Li, Y.-C. Huang and S.-W. Liu, *J. Mater. Chem. C*, 2021, **9**, 1196–1204.
29 Y. Cui, Y. Wang, J. Bergqvist, H. Yao, Y. Xu, B. Gao, C. Yang, S. Zhang, O. Inganäs, F. Gao and J. Hou, *Nat. Energy*, 2019, **4**, 768–775.
30 T. Dai, X. Li, P. Lei, A. Tang, Y. Geng, Q. Zeng and E. Zhou, *Nano Energy*, 2022, **99**, 107413.
31 A. Tang, W. Song, B. Xiao, J. Guo, J. Min, Z. Ge, J. Zhang, Z. Wei and E. Zhou, *Chem. Mater.*, 2019, **31**, 3941–3947.
32 T. Dai, A. Tang, Z. He, M. Du, P. Lei, Q. Zeng, Z. Wang, Y. Wang, S. Lu, Y. Zhong and E. Zhou, *Energy Environ. Sci.*, 2023, **16**, 2199–2211.
33 C.-Y. Liao, Y. Chen, C.-C. Lee, G. Wang, N.-W. Teng, C.-H. Lee, W.-L. Li, Y.-K. Chen, C.-H. Li, H.-L. Ho, P. H.-S. Tan, B. Wang, Y.-C. Huang, R. M. Young, M. R. Wasielewski, T. J. Marks, Y.-M. Chang and A. Facchetti, *Joule*, 2019, **4**, 189–206.
34 Y.-J. Hsieh, Y.-C. Huang, W.-S. Liu, Y.-A. Su, C.-S. Tsao, S.-P. Rwei and L. Wang, *ACS Appl. Mater. Interfaces*, 2017, **9**, 14808–14816.
35 Z. Liu and N. Wang, *Adv. Opt. Mater.*, 2019, **7**, 1900913.
36 T. Hahn, S. Tscheuschner, F.-J. Kahle, M. Reichenberger, S. Athanasopoulos, C. Saller, G. C. Bazan, T.-Q. Nguyen, P. Strohriegl, H. Bässler and A. Köhler, *Adv. Funct. Mater.*, 2017, **27**, 1604906.
37 S. Ryu, N. Y. Ha, Y. H. Ahn, J.-Y. Park and S. Lee, *Sci. Rep.*, 2021, **11**, 16781.
38 Y. Zhang, X. Li, T. Dai, D. Xu, J. Xi and X. Chen, *RSC Adv.*, 2019, **9**, 24895–24903.
39 P. P. Boix, J. Ajuria, I. Etxebarria, R. Pacios, G. Garcia-Belmonte and J. Bisquert, *J. Phys. Chem. Lett.*, 2011, **2**, 407–411.
40 G. Garcia-Belmonte, A. Guerrero and J. Bisquert, *J. Phys. Chem. Lett.*, 2013, **4**, 877–886.
41 P.-H. Lee, T.-T. Wu, K.-Y. Tian, C.-F. Li, C.-H. Hou, J.-J. Shyue, C.-F. Lu, Y.-C. Huang and W.-F. Su, *ACS Appl. Mater. Interfaces*, 2020, **12**, 45936–45949.
42 C. B. Nielsen, S. Holliday, H.-Y. Chen, S. J. Cryer and I. McCulloch, *Acc. Chem. Res.*, 2015, **48**, 2803–2812.
43 Y. Cui, H. Yao, J. Zhang, T. Zhang, Y. Wang, L. Hong, K. Xian, B. Xu, S. Zhang, J. Peng, Z. Wei, F. Gao and J. Hou, *Nat. Commun.*, 2019, **10**, 2515.
44 Z. Wang, A. Tang, H. Wang, Q. Guo, Q. Guo, X. Sun, Z. Xiao, L. Ding and E. Zhou, *Chem. Eng. J.*, 2023, **451**, 139080.
45 M. Stephen, K. Genevičius, G. Juška, K. Arlauskas and R. C. Hiorns, *Polym. Int.*, 2017, **66**, 13–25.